Mon. Not. R. Astron. Soc. **000**, 1–9 (2016) Printed 18 December 2015 (MN LATEX style file v2.2)

Dynamics and Metallicities of Red Supergiant Stars in the Young Massive Cluster NGC 2100

L. R. Patrick[1⋆], C. J. Evans[1,2], B. Davies[3], et al.
[1] *Institute for Astronomy, University of Edinburgh, Royal Observatory Edinburgh, Blackford Hill, Edinburgh EH9 3HJ, UK*
[2] *UK Astronomy Technology Centre, Royal Observatory Edinburgh, Blackford Hill, Edinburgh EH9 3HJ, UK*
[3] *Astrophysics Research Institute, Liverpool John Moores University, Liverpool Science Park ic2, 146 Brownlow Hill, Liverpool L3 5RF, UK*

Accepted Received 1; in original form

ABSTRACT
Studies of the dynamical state of young massive clusters can distinguish between models of early-time evolution. We have obtained KMOS near-IR spectroscopy for 14 red supergiant stars in the young massive star cluster NGC 2100 in the Large Magellanic Cloud (LMC). Radial velocities are estimated for the targets and the dynamical properties are estimated for the first time within this cluster. The line-of-sight velocity dispersion is shown to be flat outside of 10 pc from the cluster centre and is estimated to be $\sigma_{1D} = 2.4 \pm 0.4$ km s^{-1}. The dynamical mass of the cluster is derived as $M_{dyn} > (4.2 \pm 1.4) \times 10^4 M_{\odot}$ assuming virial equilibrium. Comparing this to the mass estimated using photometry we find reasonable agreement between the independent measurements, suggesting that the cluster is in l equilibrium and that the the velocity dispersion is not increased by binary motions.

Stellar parameters including metallicity are estimated using the J-band analysis technique which has been rigorously tested in the Local Universe. We find an average metallicity for NGC 2100 at $-0.39 \pm 0.10\,dex$, in good agreement with estimates from the literature. The age of the NGC 2100 is estimated to be 20 ± 5 Myr using isochrone ing to the RSG population, ood agreement with previous estimates.

Key words: Red Supegiants: stars. Clusters: NGC 2100. Galaxy: LMC.

1 INTRODUCTION

Young massive clusters (YMCs) are important probes of early cluster evolution and have increasingly been used as tracers of star formation in galaxies (e.g. Whitmore & Schweizer 1995; Miller et al. 1997; Zepf et al. 1999), where a YMC is defined as < 100 Myr and $> 10^4$ M$_{\odot}$ (Portegies Zwart et al. 2010). Known to contain large populations of massive stars YMCs are also important tracers of massive star formation, which is heavily clustered (de Wit et al. 2005; Parker & Goodwin 2007). In addition to being the birthplace of most of the massive stars in the Local Unive owing to the density of stars, YMCs are also the birthpl e of rich stellar exotic found in the old population of GCs

Establishing a link between YMCs and old GCs is an important, uncertain, factor in the evolution of young clusters. The vast majority of star formation occurs within clus **?**) However, observations of stars in the disk of the Milky Way show that only a small fraction of stars are actually found with clusters today (). This indicates a significant fraction of star clusters will dissolve over t

Studying the dynamical properties of YMCs is an important tool to evaluate the likelihood that a young cluster will survive to become an old GC. The end of the process of star formation, brought about by the expulsion of the most massive stars in the cluster as supernovae, expels residual gas and leaves a yo luster in a super-virial state (i.e. unstable to dissolution Lada & Lada 2003). This is key period in determining the survival of a young star cluster. Observations that the some YMCs (namely R136 in the Large Magellanic Cloud) are in dynamical equilibrium from an early age (Hénault-Brunet et al. 2012; Longmore et al. 2014) challenges the view that star clusters expand owing to gas expulsion. An alternative explanation is that these clusters expand owing to stellar e ion on a slow timescale (compared to the cross time of e cluster 10 Myr Portegies Zwart et al. 2010) and hence remain in virial equilibrium. Challenging this, (Banerjee & Kroupa 2013) suggested that the observation that YMCs are in dynamical equilibrium from an early age does not necessarily indicate that the cluster did not undergo a period of ra id gas expulsion implying that the cluster could quickly re alise on a short timescale (Banerjee & Kroupa).

Recently, the idea that globular clusters are simple

⋆ E-mail: lrp@roe.ac.uk

stellar populations has been called into question based on their kinematics, metallicities and main sequence turn-offs. Studying young massive clusters could therefore potentially help to constrain some of the proposed models for creating multiple stellar populations within GCs.

Over the last few years, medium resolution ($R > 3000$) near-IR spectroscopy has been shown to be a powerful tool to estimate stellar parameters for red supergiant stars (RSGs; Davies et al. 2010). This technique has been tested rigorously by Gazak et al. (2014) and Davies et al. (2015). The arrival of the K-band multi-object spectrograph (KMOS; Sharples et al. 2013) at the Very Large Telescope (VLT), has presented new opportunities for efficient observations of samples of RSGs in external galaxies to study their distribution and build-up of metals. Patrick et al. (2015) used KMOS observations to investigate present day metallicities of NGC 6822 (d = 0.5 Mpc) and Gazak et al. (2015) used KMOS to determine the metallicity gradient of NGC 300, a grand design spiral galaxy outside the Local Group ($d = 1.9\,Mpc$), finding striking agreement with blue supergiant stars (BSGs).

NGC 2100 is a young massive cluster in the LMC, located near the large star-forming region 30 Doradus. With an age of ∼20 Myr (Elson 1991; Niederhofer et al. 2015), and a mass of $4.6 \times 10^4 M_\odot$ (McLaughlin & van der Marel 2005, assuming King (1966) profiles), NGC 2100 falls within the mass and age range where the infrared cluster light is dominated by RSGs (Gazak et al. 2013), supported by the large number of RSGs identified within this cluster (e.g. Figure 1).

NGC 2100 is not a cluster in isolation. It is located in one of the most actively star-forming regions within the Local Group of galaxies. At ∼20 Myr old, the most massive members of this star cluster will have already exploded as supernovae. This will have a profound effect on the surrounding gas and dust, and has potentially shaped the surrounding LMC 2 supershell (see Points et al. 1999).

In this study we estimate stellar parameters from KMOS spectroscopy for 14 RSGs in the vicinity of the young massive cluster NGC 2100. Section 2 we describe the observations and data reduction, and in section 3 we detail our results, focusing on radial velocities of the target stars where we derive the line-of-sight velocity dispersion, the dynamical mass of NGC 2100 and the stellar parameters. Our results are discussed in Section 4 and conclusions are presented in Section 5.

2 OBSERVATIONS AND DATA REDUCTION

2.1 Target Selection

- Ben, could you write a few lines here?

2.2 KMOS Observations

These observations were obtained as part of the KMOS Guaranteed Time Observing (PI: Evans) and were conducted in March 2015. The observations consisted of 8×10 s exposures taken with the YJ grating with sky offset exposures (S) interleaved between the object (O) exposures in an O, S, O observing pattern. In addition, a standard set of

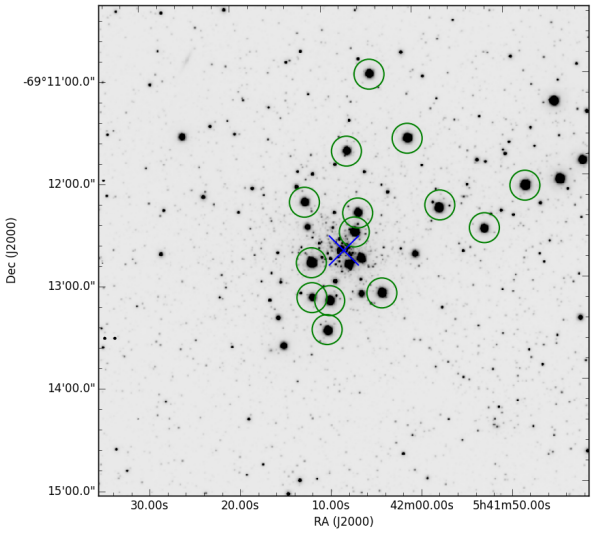

Figure 1. Positions of the NGC 2100 KMOS targets overlaid on a VISTA J-band image. Green circles indicate KMOS targets. The cluster centre has been marked by a blue cross.

KMOS calibration frames were obtained as well as observations of HD 51506 (B5) as the telluric standard star. Seeing conditions were stable at 1.0 arcseconds for the course of the observations.

The KMOS/esorex standard routines (SPARK; Davies et al. 2013) were used to calibrate and reconstruct the data cubes. Telluric correction was performed using the 24-arm telluric correction routine (described in detail by Patrick et al. 2015). Briefly, corrections to the standard telluric recipe are put in place to correct for slight differences in wavelength calibration between the telluric and science spectra. This is implemented using an iterative cross-correlation approach. Additionally, differences in the strength of the telluric features are corrected by applying a simple scaling using the equation,

$$T_2 = (T_1 + c)/(1 + c) \quad (1)$$

where T_2 is the scaled telluric-standard spectrum, T_1 is the uncorrected telluric-standard spectrum and c is the scaling parameter which is varied from $c = -0.5$ to $c = 0.5$ in increments of 0.02. The best c value is chosen based on the overall standard deviation of the spectrum, i.e. the c value producing the smallest σ is selected. Once these corrections are accounted for, the science spectra are divided by the appropriate telluric spectrum for that particular IFU.

3 RESULTS

3.1 Radial velocities

Radial velocities are estimated using an iterative cross-correlation method. To ensure systematic shifts are removed, the observed spectra are first cross-correlated against a spectrum of the Earth's atmosphere, taken from the ISAAC web-

Table 1. Summary of VLT-KMOS targets in NGC 2100.

ID	S/N	α (J2000)	δ (J2000)	B	V	I	J	H	K_s	RV (km s^{-1})	Notes
0207-0134568	318	05:41:47.873	-69:12:05.959	16.488	13.749	9.769	9.525	8.603	8.200	238.9±1.1	
0207-0134683	198	05:41:52.430	-69:12:30.410	16.430	14.267	11.970	10.413	9.526	9.155	238.7±2.2	
0207-0134811	202	05:41:57.286	-69:12:16.480	14.074	13.019	11.170	9.811	9.036	8.738	239.8±1.3	C2
0207-0134979	252	05:42:03.877	-69:13:07.410	15.624	13.579	11.410	9.839	8.996	8.740	240.4±1.5	
0207-0135059	196	05:42:06.348	-69:12:20.150	...	...	11.810	10.371	9.480	9.159	245.0±2.9	B17
0207-0135069	256	05:42:06.764	-69:12:31.245	15.643	13.675	11.390	9.977	9.150	8.807	239.5±2.3	
0207-0135150	240	05:42:09.647	-69:13:11.263	15.367	13.383	11.370	9.976	9.136	8.841	240.8±3.2	
0207-0135162	250	05:42:10.001	-69:13:28.210	16.060	13.827	11.580	10.021	9.150	8.823	240.2±1.4	C32
0207-0135205	304	05:42:11.574	-69:12:48.770	16.327	14.033	11.450	9.557	8.617	8.264	238.0±1.9	
0207-0135206	151	05:42:11.592	-69:13:09.257	16.165	14.272	12.340	10.943	10.090	9.788	241.4±2.5	
0207-0135220	195	05:42:12.182	-69:12:13.144	15.483	13.606	11.750	10.440	9.622	9.335	246.0±3.3	
0208-0135292	262	05:42:00.722	-69:11:36.925	15.579	13.674	9.421	9.900	9.017	8.683	242.2±3.1	
0208-0135383	211	05:42:04.762	-69:10:58.816	15.550	13.800	12.770	10.319	9.427	9.159	245.7±2.3	
0208-0135446	201	05:42:07.435	-69:11:43.692	15.531	13.661	11.780	10.482	9.610	9.351	242.4±3.2	

Photometric data taken from the SIMBAD database. Typical errors on photometric data: 0.026, 0.014, 0.04, 0.024, 0.026, 0.022 respectively. Near-IR data taken from 2MASS.

pages, which is at a much higher resolution than that of the KMOS observations. This cross-correlation is performed in the $1.15-1.17\,\mu$m region as this is where the telluric features dominate. This shift is then applied to the $1.16-1.22\,\mu$m region, i.e. where the radial velocity is estimated.

Once the observed spectra are on a consistent wavelength solution, an initial guess of the radial velocity is estimated by cross-correlating the science spectra with an appropriate synthetic RSG spectrum in the $1.17-1.21\,\mu$m region. This wavelength regime is selected based on the dominance of atomic features in the RSG spectrum at these wavelengths. To increase reliability, this initial guess is improved upon by using five carefully selected groups of stellar absorption lines centred on some of the strongest atomic features in this region. These lines and regions are known to be not affected by telluric absorption. Figure 2 illustrates the selected features used for the analysis.

Radial velocities are independently calculated for each region by means of iterative cross-correlation. This results in five estimates of the radial velocity for each star which are then compared and any region which produces a radial velocity which is an obvious outlier to the distribution is rejected. The final radial velocity for each star is the mean of the distribution resulting from the (non-rejected) regions. Not rejecting these outliers has the effect of increasing the error on each individual radial velocity but it does not alter the mean of the sample or the deviation significantly ($< RV > \; = \; 244 \pm 3\,\mathrm{km\ s^{-1}}$). The error on this mean is calculated by taking the standard deviation of the data, normalised by the number of regions used ($err = \sigma/N_{regions}$). This method is known to work well for KMOS spectra (Lapenna et al. 2015; Patrick et al. 2015).

Figure 3 shows all stellar radial velocity estimates as a function of distance from the centre of the cluster, alongside the systemic radial velocity of the LMC (green dashed line). Given the low dispersion of the radial velocity measurements for the KMOS targets, we confirm that all of the targets within this sample are members of NGC 2100. Table 2 details previous measurements of radial velocities within this cluster.

Recently, Evans et al. (2015) used AAOmega to measure radial velocities of massive stars within LMC, which included two sources in NGC 2100: star 407 (O9.5 II $258.5 \pm 3.4\,\mathrm{km\ s^{-1}}$) and star 408 (B3 Ia; $250.6 \pm 1.3\,\mathrm{km\ s^{-1}}$).

Jasniewicz & Thevenin (1994) measured radial velocities for four RSGs in NGC 2100 (B17, C2, C32 and C34, using the nomenclature of Robertson 1974). Three of these stars have been observed with KMOS in the present study (207-0135059; B17, 207-0134811; C2 and 207-0135162; C32). A comparison between the radial velocities estimated in JT94 with those presented here highlights the discrepancy between the measurements. The average offset between the three stars which are common to the samples is $-18.3 \pm 5.2\,\mathrm{km\ s^{-1}}$. However, previous stellar radial velocity estimates using KMOS have shown small, not-statistically significant offsets when compared with previous measurements (Lapenna et al. 2015; Patrick et al. 2015). Regardless, we can not ignore the possibility that there exists some systematic offset in the radial velocity estimated in this study.

Freeman et al. (1983) compiled integrated-light radial velocities from Andrews & Lloyd Evans (1972) and Ford (1970) to define an average of $267 \pm 13\,\mathrm{km\ s^{-1}}$for NGC 2100. Whereas Smith & Weedman (1971), measured the radial velocity of the HII gas of NGC 2100 as $282.2 \pm 2.5\,\mathrm{km\ s^{-1}}$.

3.2 Velocity Dispersion

An upper limit to the line-of-sight velocity dispersion is calculated using the equations,

$$\mu = \frac{1}{\sum_i 1/\sigma_i^2} \sum_i \frac{RV_i}{\sigma_i}, \tag{2}$$

$$Var = \frac{1}{\sum_i 1/\sigma_i^2} \sum_i \frac{(RV_i - \mu)^2}{\sigma_i^2}, \tag{3}$$

$$\sigma_{1D} = \sqrt{Var \frac{N}{N-1}}, \tag{4}$$

where σ_i is the uncertainty on the radial velocity measurement RV_i, μ is the weighted mean and N is the number of stars in the sample. Figure 4 shows the line-of-sight velocity dispersion profile for RSGs in NGC 2100. The uncertainties in this figure are defined as the standard deviation of the radial velocities within the given distance, normalised by the number of measurements in the sample. We see that the dispersion is consistent with a flat profile with a value of $\sim$2.5 km s^{-1}. The apparent outlier at $\sim$5 pc is owing to

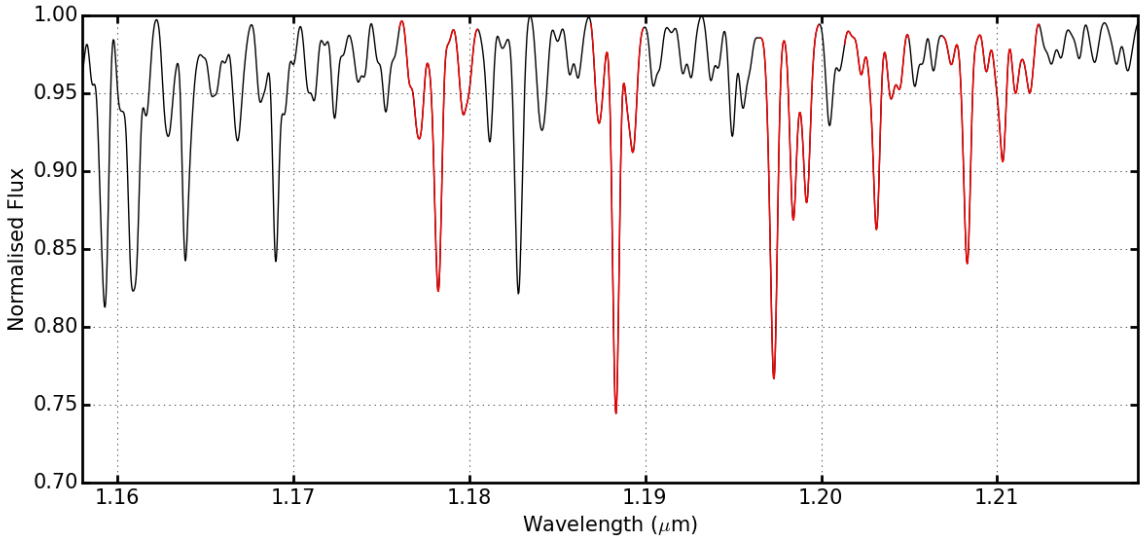

Figure 2. Synthetic RSG spectrum used calculate the radial velocities for programme stars. Red regions illustrate those used to cross-correlate the observed spectra with this synthetic spectrum. These regions provide consistent results with an average dispersion between the five regions of of 2.3 km s^{-1}.

Table 2. Previous radial velocity measurements in NGC 2100.

ID	ID in current study	RV (km s^{-1})	Reference	Notes
407	—	258.5 ± 3.4	Evans et al. (2015)	O9.5 II
408	—	250.6 ± 1.3	Evans et al. (2015)	B3 Ia
B17	207-0135059	$255 \pm 8/245.0 \pm 2.9$	Jasniewicz & Thevenin (1994)	
C2	207-0134811	$270 \pm 8/239.8 \pm 1.3$	Jasniewicz & Thevenin (1994)	
C32	207-0135162	$260 \pm 8/240.2 \pm 1.4$	Jasniewicz & Thevenin (1994)	
C34	—	265 ± 8	Jasniewicz & Thevenin (1994)	
NGC 2100	—	$280 \pm 10(16)$	Andrews & Lloyd Evans (1972)	Whole cluster
NGC 2100	—	282.2 ± 2.5	Smith & Weedman (1971)	Gas
NGC 2100	—	253 ± 17	Ford (1970)	

Value in braces is the error defined from Freeman et al. (1983).

the low number statistics within this radius. Thus, we adopt $\sigma_{1D} = 2.4 \pm 0.4$ km s^{-1}, where this uncertainty is the average of all the σ_{1D} measurements in Figure 4, as an upper limit on the line-of-sight velocity dispersion profile of NGC 2100. A discussion on how binarity affects this distribution is given in Section 4.2.

3.3 Dynamical Mass

Using σ_{1D} as an upper limit on the velocity distribution, one can calculate the dynamical mass of the cluster using the virial equation,

$$M_{dyn} = \frac{\eta \sigma_{1D}^2 r_{eff}}{G}, \quad (5)$$

where M_{dyn} is the virial mass, $\eta = 6 r_{vir}/r_{eff} = 9.75$ providing the density profile of the cluster is sufficiently steep (Portegies Zwart et al. 2010). However, NGC 2100 has a relatively shallow density profile ($\gamma = 2.44 \pm 0.14$; Mackey & Gilmore 2003) which means $\eta > 9.75$ and therefore the estimate of M_{dyn} is knowingly an overestimate. Using $\sigma_{1D} = 2.4 \pm 0.4$ km s^{-1}and equation 5, the dynamical mass of NGC 2100 is $M_{dyn} = (5.8 \pm 2.0) \times 10^4 M_\odot$. Comparing this to the photometric mass $M_{phot} = (2.3 \pm 1.0) \times 10^4 M_\odot$ (McLaughlin & van der Marel 2005) we see that the dynamical mass appears to be a slight overestimate. Gieles et al. (2010) explain this discrepancy by demonstrating that binary motions can increase the measured velocity dispersion profile. Hénault-Brunet et al. (2012) noted that had binarity been neglected they would have measured a σ_{1D} a factor of five higher for R136. However, the mean lifetime for RSGs within binary systems is significantly decreased (Eldridge et al. 2008). These authors also noted that where mass transfer occurs, the number of RSGs drastically decreases. We can therefore expect that the numbers of RSGs in close binary systems are very small (Davies et al. 2009). The fraction of RSGs in longer period binary systems is more uncertain, however, these systems would increase the line-of-sight velocity dispersion to a lesser degree.

Assuming that the population of RSGs we observe is entirely single leads to the conclusion that the only factor affecting the estimation of M_{dyn} is the η parameter. Using a lower estimate of $\eta = 7.0$ (estimated from Fig. 4a in Portegies Zwart et al. 2010), $M_{dyn} = (4.2 \pm 1.4) \times 10^4 M_\odot$ which accounts for the discrepancy between the measured

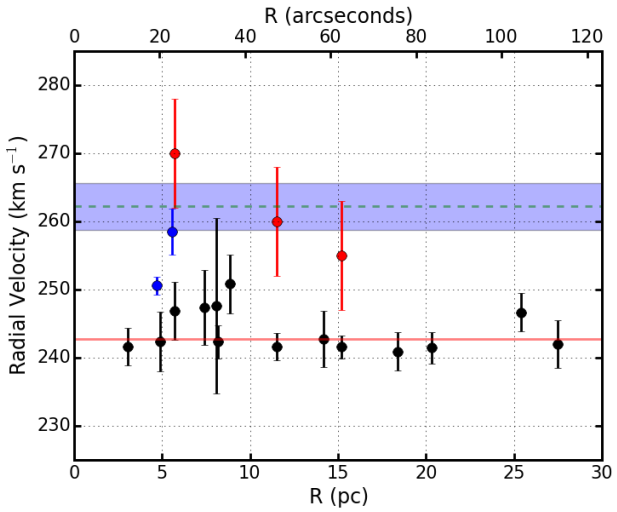

Figure 3. Radial velocities of KMOS targets shown as a function of distance from the cluster centre. Green dashed line shows the LMC systemic velocity with the error highlighted by the blue shaded region (262.2 ± 3.4 km s^{-1}; McConnachie 2012) and the solid red line shows the mean of the sample (242.7 ± 2.4 km s^{-1}). Blue points show the two young stars studied in Evans et al. (2015) and red points show previous estimates for three of the targets (Jasniewicz & Thevenin 1994).

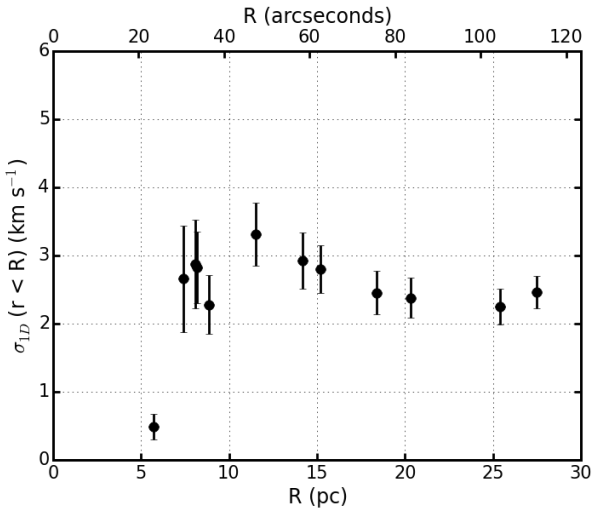

Figure 4. Observed line-of-sight velocity dispersion as a function of the distance from the centre of NGC 2100.

masses. As we can account for the differences in the mass measurements using just the η parameter, this implies that the assumption that the RSGs in our sample are single objects is correct.

3.4 Stellar Parameters

Stellar parameters are estimated using the J-band analysis technique described initially in Davies et al. (2010) and tested rigorously by Gazak et al. (2014) and Davies et al. (2015). These studies show that using a narrow spectral window within the *J*-band one can accurately derive overall metallicities ([Z]) to better than $\pm 0.15\,dex$ at the resolution of KMOS observations with S/N $\geqslant$ 100. Patrick et al. (2015) built on this by demonstrating the feasibility of this technique using KMOS spectra.

Table 3. Model grid used for analysis.

Model Parameter	Min.	Max.	Step size
T_{eff} (K)	3400	4400	100
[Z] (dex)	−1.0	1.0	0.1
log g (cgs)	−1.00	1.00	0.25
ξ (km s^{-1})	1.0	5.0	0.2

The analysis uses synthetic RSG spectra, extracted from MARCS model atmospheres (Gustafsson et al. 2008), computed with corrections for non-local thermodynamic equilibrium for stellar lines from titanium, iron, silicon and magnesium (Bergemann et al. 2012, 2013, 2015). The parameter ranges for the grid of synthetic RSG spectra are listed in Table 3. The synthetic spectra are compared with observations using a χ-squared minimisation approach where the synthetic spectra are degraded to the resolution and sampling of the observations.

Estimated stellar parameters are listed in Table 4. Reliable parameters could not be estimated for two stars (0207-0135059 and 0207-0135206). Figure 5 shows the observed KMOS spectra (black) along with each best-fitting model spectrum (red). The average metallicity for the 14 stars within NGC 2100 is $-0.39 \pm 0.10\,dex$ and the distribution of metals with respect to distance from the cluster centre is shown in Figure 6.

The average metallicity in NGC 2100 compares well to estimates of the cluster metallicity using isochrone fitting to the optical colour-magnitude diagram ($-0.34\,dex$; Niederhofer et al. 2015). The only other estimate of stellar metallicity within this cluster comes from Jasniewicz & Thevenin (1994) who estimated metallicities using optical spectroscopy of four RSGs. These authors found an average metallicity for NGC 2100 of $-0.32 \pm 0.03\,dex$, which our estimate agrees well with. We find that there are three targets in common with our study: B17, C2, C32 (using the Robertson 1974, nomenclature). **Comparing results we find B17 has a spuriously high metallicity for the sample. However, this spectrum displays no obvious features of a poor telluric correction or sky subtraction with a signal-to-noise ratio far exceeding that of our minimum threshold to perform the analysis. C34 & C2 have a microturblence value on the edge of the grid.**

Using the same analysis technique as in this study, Davies et al. (2015) estimate metallicities for nine RSGs within the LMC, finding an average value of $-0.37 \pm 0.14\,dex$ which again, our estimate agrees well with.

4 DISCUSSION

4.1 Stellar Parameters

Luminosities have been estimated using the bolometric correction in Davies et al. (2013) and a H-R diagram for the clusters is presented in Figure 7. Overlaid on this H-R diagram are SYCLIST stellar isochrones for SMC-like (solid lines,

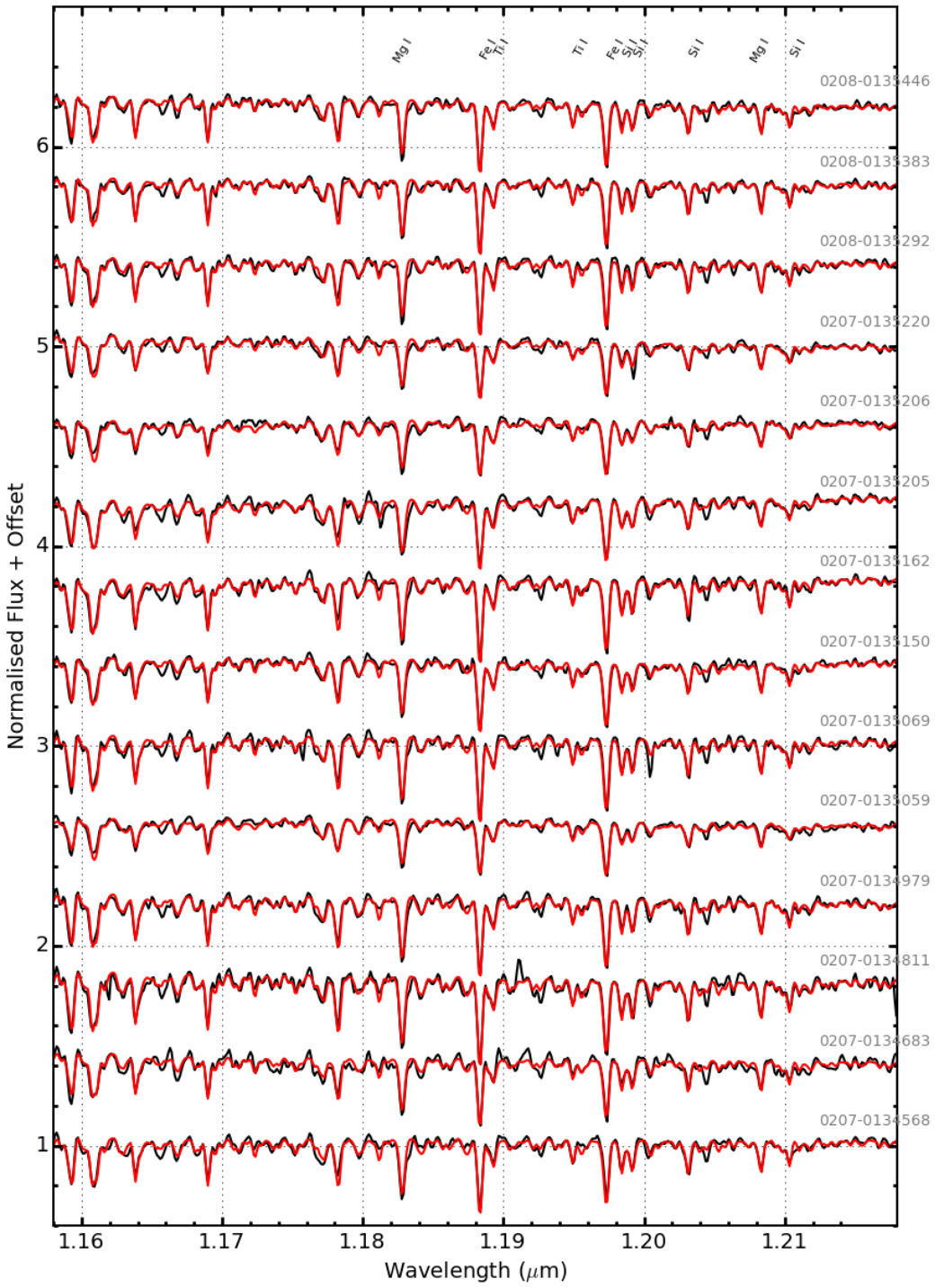

Figure 5. KMOS spectra of the NGC 2100 RSGs and their associated best-fit model spectra (black and red lines, respectively). The lines used for the analysis from left-to-right by species are: Fe I λλ1.188285, 1.197305, Si I λλ1.198419, 1.199157, 1.203151, 1.210353, Ti I λλ1.189289, 1.194954.

Table 4. Physical parameters for the NGC 2100 KMOS targets

Target	IFU	ξ (km s^{-1})	[Z]	log g	T$_{eff}$ (K)	Notes
0207-0134568	7	3.6 ± 0.19	-0.39 ± 0.07	0.12 ± 0.12	4048 ± 63	
0207-0134683	9	3.5 ± 0.18	-0.439± 0.09	0.42 ± 0.18	4002 ± 26	
0207-0134811	6	5.0 ± 0.10	-0.38 ± 0.07	0.18 ± 0.13	3994 ± 43	C2
0207-0134979	12	4.6 ± 0.14	-0.47 ± 0.05	0.24 ± 0.13	3894 ± 50	
0207-0135059	24	2.5 ± 0.47	0.01 ± 0.27	0.45 ± 0.11	3773 ± 132	B17
0207-0135069	10	5.0 ± 0.10	-0.48 ± 0.05	0.24 ± 0.13	3904 ± 50	
0207-0135150	14	3.7 ± 0.20	-0.34 ± 0.12	0.06 ± 0.21	3767 ± 73	
0207-0135162	11	5.0 ± 0.10	-0.44 ± 0.09	0.16 ± 0.20	3948 ± 44	C32
0207-0135205	20	3.8 ± 0.19	-0.21 ± 0.09	-0.01 ± 0.17	3906 ± 68	
0207-0135206	18	2.1 ± 0.24	0.34 ± 0.08	0.75 ± 0.13	3800 ± 50	
0207-0135220	22	3.3 ± 0.21	-0.25 ± 0.12	0.36 ± 0.25	4040 ± 54	
0208-0135292	4	4.2 ± 0.23	-0.44 ± 0.10	0.17 ± 0.10	3784 ± 76	
0208-0135383	3	4.1 ± 0.20	-0.45 ± 0.09	0.48 ± 0.10	3893 ± 50	
0208-0135446	2	4.0 ± 0.21	-0.37 ± 0.09	0.48 ± 0.13	3864 ± 50	

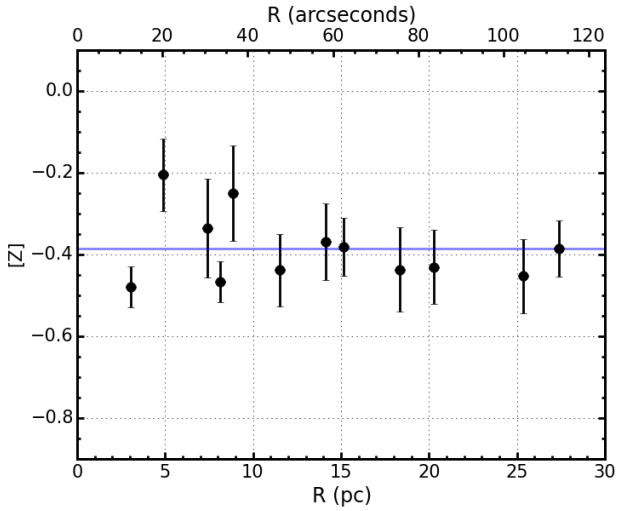

Figure 6. Estimated metallicities shown against distance from the centre of the cluster where the solid blue line denotes the mean of the sample $-0.39 \pm 0.10\,dex$.

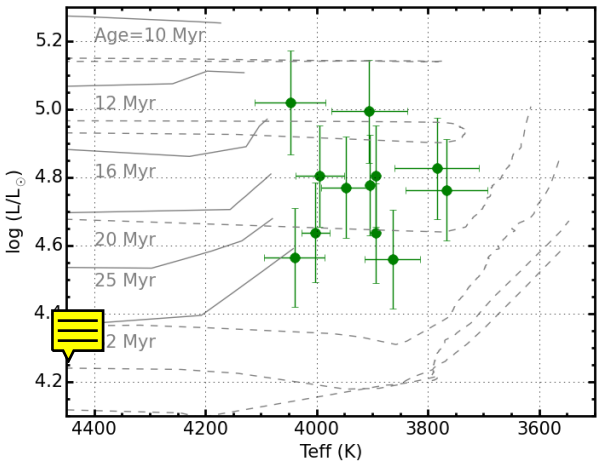

Figure 7. H-R diagram for 12 RSGs in NGC2100. Cluster isochrones for solar (dashed lines Ekström et al. 2012) and SMC-like (solid lines Georgy et al. 2013) metal abundances, where stellar rotation is 40% of the break-up velocity, are shown for ages of 10-32 Myr.

Georgy et al. 2013) and solar-like (dashed lines, Ekström et al. 2012) models where stellar rotation is 40% of break-up velocity. Even though the temperatures covered by the SMC-like models do not accurately represent the distribution of temperatures observed in this study, it remains useful to fit the data using these models to estimate an age for NGC 2100. The Solar-like models (dashed) demonstrate that increasing the metallicity of the sample a) decreases the temperatures of the RSGs (something which is not observed by Patrick et al. 2015), b) induces a blue-ward evolution for the youngest models and c) decreases the luminosity for the oldest models.

Davies et al. (2015) estimated stellar parameters for nine RSGs throughout the LMC using the same methodology as in this study. In Figure 8 we compare the effective temperatures and metallicities from NGC 2100 with those derived for RSGs elsewhere in the LMC. We find excellent agreement in the distribution of temperatures from the two studies, with the average agreeing well. The range in [Z] from the LMC population is slightly larger than that of the NGC 2100 RSGs, which is expected when comparing a star cluster with an entire galaxy, however the averages for the two studies agree very well.

4.2 Velocity Dispersion and Dynamical Mass

This study represents the first estimate of the line-of-sight velocity dispersion profile for NGC 2100. Comparing this estimate with that of other young massive clusters in the Local Universe is useful to ascertain whether this cluster shares similar properties to other more well studied young massive clusters. We find the dynamical properties NGC 2100 are well matched by other clusters with similar masses and ages, particularly so with RSGC02, a Galactic young massive cluster. A comparison with a small sample of Local Group YMCs reveals the trend that very young massive clusters (defined as 1-3 Myr by Banerjee & Kroupa 2015) have a larger line-of-sight velocity dispersion which relaxes to $\sim$3 km s^{-1}at 10-100 Myr.

5 CONCLUSIONS

Using KMOS spectra of 14 RSGs in NGC 2100 we have for the first time estimated the dynamical properties of this young massive cluster. Radial velocities have been estimated

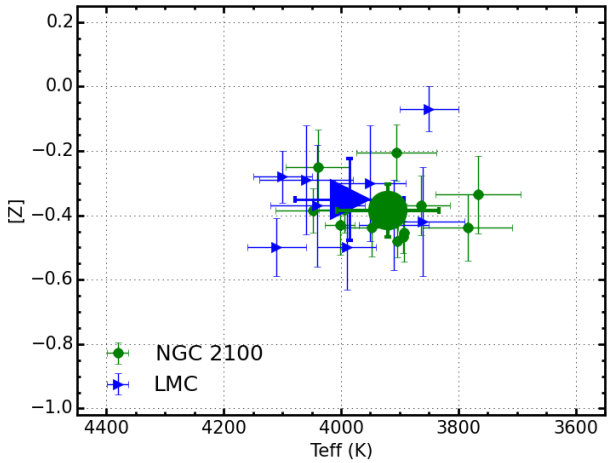

Figure 8. Estimated metallicities for NGC 2100 RSGs in this study shown against effective temperature (green dots). For comparison we show the distribution of LMC RSGs in Davies et al. (blue triangles 2015). This demonstrates the remarkable agreement between the effective temperature ranges and averages for RSGs within these two samples.

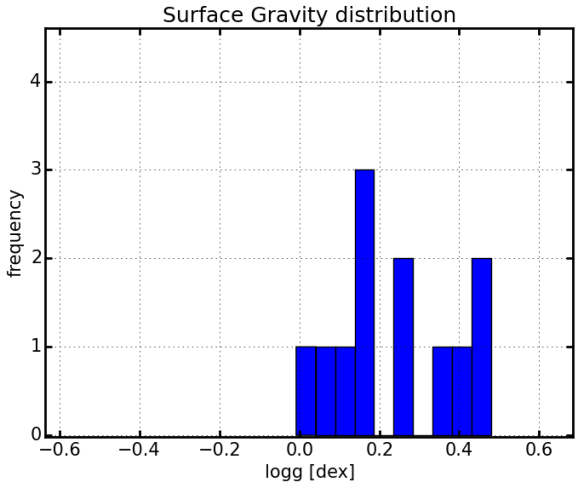

Figure 9. Histogram showing the range of surface gravities estimated. Average value $0.24 \pm 0.15\,dex$. For Illustration only.

using KMOS, to a precision of $\sim 1\,\mathrm{km\ s^{-1}}$, demonstrating that this instrument can be used to study the dynamical properties of star clusters in external galaxies.

The line-of-sight velocity dispersion profile has been estimated in Figure 4 and has been shown to be flat outside 10 pc from the cluster centre. A low velocity dispersion of $\sigma_{1D} = 2.4 \pm 0.4\,\mathrm{km\ s^{-1}}$has been adopted and NGC 2100 has therefore been shown to be in virial equilibrium. This adds evidence to the theory that young star clusters appear to remain in virial equilibrium from an early age and hence expand owing to stellar evolution on a relatively slow timescale (10 Myr Portegies Zwart et al. 2010). We compare the velocity dispersion profile estimated here to that of other young massive clusters in the LMC and the Galaxy and find that the distribution of velocity dispersions is consistent with this expansion.

Characterisation of the velocity dispersion profile for the cluster allows for the first time the dynamical mass to be estimated (assuming virial equilibrium) as $log(M_{dyn}/M_{\odot}) > 4.8$. A discussion of the appropriate value of η for this cluster is detailed in Section 3.3.

We estimate stellar parameters for the RSGs in NGC 2100 using the J-band analysis technique (Davies et al. 2010) for all targets within the sample. We find the average metallicity for RSGs in NGC 2100 is $-0.30 \pm 0.11\,dex$, which agrees well with previous studies within this cluster. We construct a H-R diagram of RSGs within NGC 2100 and estimate the age of the cluster using isochrones fitting (Ekström et al. 2012; Georgy et al. 2013) to be 20 ± 5 Myr, in good agreement with the estimate for this cluster from Niederhofer et al. (2015).

ACKNOWLEDGEMENTS

...

REFERENCES

Andrews, P. J., & Lloyd Evans, T. 1972, MNRAS, 159, 445
Banerjee, S., & Kroupa, P. 2013, ApJ, 764, 29
Banerjee, S., & Kroupa, P. 2015, arXiv:1512.03074
Bergemann, M., Kudritzki, R.-P., Plez, B., et al. 2012, ApJ, 751, 156
Bergemann, M., Kudritzki, R.-P., Würl, M., et al. 2013, ApJ, 764, 115
Bergemann, M., Kudritzki, R.-P., Gazak, Z., Davies, B., & Plez, B. 2015, ApJ, 804, 113
Clark, J. S., Negueruela, I., Crowther, P. A., & Goodwin, S. P. 2005, A&A, 434, 949
Crowther, P. A., Schnurr, O., Hirschi, R., et al. 2010, MNRAS, 408, 731
Davies, B., Figer, D. F., Kudritzki, R.-P., et al. 2007, ApJ, 671, 781
Davies, B., Origlia, L., Kudritzki, R.-P., et al. 2009, ApJ, 696, 2014
Davies, B., Kudritzki, R.-P., & Figer, D. F. 2010, MNRAS, 407, 1203
Davies, B., Kudritzki, R.-P., Plez, B., et al. 2013, ApJ, 767, 3
Davies, B., Kudritzki, R.-P., Gazak, Z., et al. 2015, ApJ, 806, 21
Davies, R. I., Agudo Berbel, A., Wiezorrek, E., et al. 2013, A&A, 558, A56
de Koter, A., Heap, S. R., & Hubeny, I. 1998, ApJ, 509, 879
de Wit, W. J., Testi, L., Palla, F., & Zinnecker, H. 2005, A&A, 437, 247
Ekström, S., Georgy, C., Eggenberger, P., et al. 2012, A&A, 537, A146
Eldridge, J. J., Izzard, R. G., & Tout, C. A. 2008, MNRAS, 384, 1109
Elson, R. A. W. 1991, ApJS, 76, 185
Evans, C. J., Lennon, D. J., Smartt, S. J., & Trundle, C. 2006, A&A, 456, 623

Evans, C. J., Taylor, W. D., Hénault-Brunet, V., et al. 2011, A&A, 530, A108
Evans, C. J., van Loon, J. T., Hainich, R., & Bailey, M. 2015, arXiv:1508.03490
Ford, H., 1970, PhD. Thesis, University of Wisconsin.
Freeman, K. C., Illingworth, G., & Oemler, A., Jr. 1983, ApJ, 272, 488
Gazak, J. Z., Bastian, N., Kudritzki, R.-P., et al. 2013, MNRAS, 430, L35
Gazak, J. Z., Davies, B., Kudritzki, R., Bergemann, M., & Plez, B. 2014, ApJ, 788, 58
Gazak, J. Z., Davies, B., Bastian, N., et al. 2014, ApJ, 787, 142
Gazak, J. Z., Kudritzki, R., Evans, C., et al. 2015, ApJ, 805, 182
Georgy, C., Ekström, S., Eggenberger, P., et al. 2013, A&A, 558, A103
Gieles, M., Sana, H., & Portegies Zwart, S. F. 2010, MNRAS, 402, 1750
Gratton, R. G., Lucatello, S., Carretta, E., et al. 2012, A&A, 539, A19
Gustafsson, B., Edvardsson, B., Eriksson, K., et al. 2008, A&A, 486, 951
Hénault-Brunet, V., Evans, C. J., Sana, H., et al. 2012, A&A, 546, A73
Jasniewicz, G., & Thevenin, F. 1994, A&A, 282, 717
King, I. R. 1966, AJ, 71, 64
Lada, C. J., & Lada, E. A. 2003, ARA&A, 41, 57
Lapenna, E., Origlia, L., Mucciarelli, A., et al. 2015, ApJ, 798, 23
Longmore, S. N., Kruijssen, J. M. D., Bastian, N., et al. 2014, Protostars and Planets VI, 291
Mackey, A. D., & Gilmore, G. F. 2003, MNRAS, 338, 85
Massey, P., & Hunter, D. A. 1998, ApJ, 493, 180
McConnachie, A. W. 2012, AJ, 144, 4
McLaughlin, D. E., & van der Marel, R. P. 2005, ApJS, 161, 304
Miller, B. W., Whitmore, B. C., Schweizer, F., & Fall, S. M. 1997, AJ, 114, 2381
Niederhofer, F., Hilker, M., Bastian, N., & Silva-Villa, E. 2015, A&A, 575, A62
Parker, R. J., & Goodwin, S. P. 2007, MNRAS, 380, 1271
Patrick, L. R., Evans, C. J., Davies, B., et al. 2015, ApJ, 803, 14
Points, S. D., Chu, Y. H., Kim, S., et al. 1999, ApJ, 518, 298
Portegies Zwart, S. F., McMillan, S. L. W., & Gieles, M. 2010, ARA&A, 48, 431
Robertson, J. W. 1974, A&AS, 15, 261
Sharples, R., Bender, R., Agudo Berbel, A., et al. 2013, The Messenger, 151, 21
Smith, M. G., & Weedman, D. W. 1971, ApJ, 169, 271
Whitmore, B. C., & Schweizer, F. 1995, AJ, 109, 960
Zepf, S. E., Ashman, K. M., English, J., Freeman, K. C., & Sharples, R. M. 1999, AJ, 118, 752